

## Axis Ratios of Water Drops Levitated in a Vertical Wind Tunnel

B. K. JONES AND J. R. SAYLOR

*Department of Mechanical Engineering, Clemson University, Clemson, South Carolina*

(Manuscript received 5 January 2009, in final form 12 June 2009)

### ABSTRACT

The shapes of falling raindrops are often significantly altered by drop oscillations, complicating dual-polarization radar methods that rely on a predictable, monotonic variation of drop axis ratio  $\alpha$  with equivalent volume drop diameter  $d$ . This oscillation behavior varies with  $d$  so that time-averaged shapes, which are determined by oscillation mode, sometimes deviate from the  $d$ -dependent quiescent shape. The literature identifies a predominance of particular oscillation modes at discrete  $d$ , as well as the onset of oscillations at  $d \approx 1$  mm; however, the specific mechanisms of this phenomenon are unknown. In the present work, measurements of drop axis ratio  $\alpha$  were obtained from observations of drops levitated in a vertical wind tunnel. Discordance of the present data with the literature suggests a correlation between oscillation mode and fall trajectory, as well as a steady-state mechanism for the excitation of specific modes for  $d = 1.3$ – $3$ -mm drops.

### 1. Introduction

The use of radar instrumentation for the remote sensing of rain has become an essential aspect of meteorological science. Temporally and spatially, the resolution and range of weather radars are superior to any other method of precipitation measurement. Rain-rate  $r$  measurement using traditional single-polarization radar involves transmitting a microwave signal and measuring the intensity of the echo backscattered by raindrops. This intensity determines a reflectivity factor  $Z$ , which is used to estimate parameters of the drop size distribution  $N(d)$ , where  $d$  is the drop diameter of an equivalent volume sphere, usually modeled as an exponential distribution of the form

$$N(d) = N_o e^{-\Lambda d}, \quad (1)$$

with the two unknown parameters  $\Lambda$  ( $\text{cm}^{-1}$ ) and  $N_o$  ( $\text{m}^{-3} \text{cm}^{-1}$ ). The problem of accurately determining these two unknowns from the single measurable  $Z$  has historically been approached using various empirical techniques (Marshall and Palmer 1948; Ulbrich 1986), but these methods are problematic and sometimes introduce measurement error comparable in magnitude to

trends of interest (Musgrove and Brook 1975; Doviak and Zrnica 1984).

To circumvent this error and the single-measurable problem, dual-polarization radar has been developed to provide a second measurable for the calculation of  $N(d)$ . The most common implementation of this technique measures the backscatter signals of two orthogonal radar waves polarized in vertical and horizontal orientations. The ratio of these two signals varies with  $d$  because of the aspherical shapes exhibited by falling raindrops and the variation of this shape with drop size, which is illustrated in Fig. 1. This variation is typically characterized by the ratio  $\alpha$  defined as

$$\alpha = \frac{v}{h}, \quad (2)$$

where  $v$  and  $h$  are the vertical and horizontal chords of the drop, respectively. Because larger drops exhibit more oblate shapes than smaller drops, as shown in Fig. 1,  $\alpha$  decreases with increasing  $d$ . This monotonic relationship means that values of the dual-polarization backscatter ratio vary proportionally with the diameter of falling drops, effectively providing a second measurable for the calculation of  $N(d)$ .

The silhouettes shown in Fig. 1 illustrate the shapes of quiescent raindrops and result from a balance of internal fluid forces and aerodynamic pressure in the flow region outside the drop. Observations of the average axis ratio  $\bar{\alpha}$  of falling drops, however, have shown that drops larger

*Corresponding author address:* Brian K. Jones, 1162 Ben Hill Blvd., Nolensville, TN 37135.  
E-mail: brian.k.jones@gmail.com

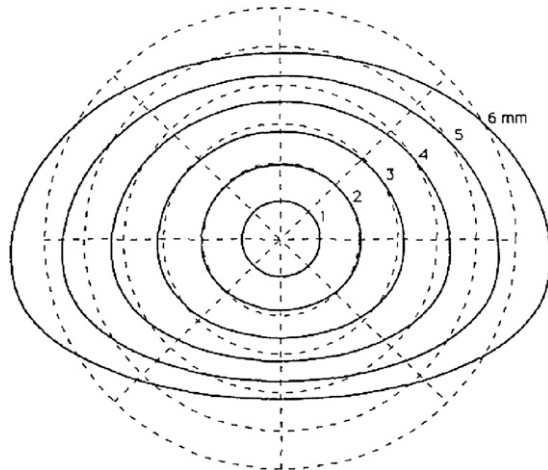


FIG. 1. Quiescent drop shapes. Figure from Beard and Chuang (1987).

than 1 mm tend to oscillate during free-fall and exhibit average shapes that are distorted significantly from the quiescent shapes shown in Fig. 1 (Beard and Kubesh 1991; Chandrasekar et al. 1988; Andsager et al. 1999). These oscillations have complicated efforts to establish a predictable relationship between  $d$  and  $\alpha$  (or  $\bar{\alpha}$ ), compromising the improvements in accuracy afforded by the dual-polarization technique.

Rayleigh (1879) found that oscillations occur at  $n$  discrete harmonic frequencies (ranging from 350–30 Hz for  $d \approx 1$ –5 mm raindrops) in  $m = n + 1$  discrete modes. More recently, Beard and Kubesh (1991) examined  $\alpha$  data obtained from images of falling drops and combined these with a theoretical analysis of modal shapes to suggest that certain modes are more common at particular drop sizes. This work revealed that for axisymmetric modal shapes ( $n, m = 2, 0$ ) distortions are such that  $\alpha$  measurements of oscillating drops vary equally above and below the quiescent  $\alpha$ ; thus  $\bar{\alpha}$  measurements for these modes are very near that of the quiescent shape. For one particular mode (transverse;  $n, m = 2, 1$ ), however, distortions are such that  $\alpha$  only varies above the quiescent, so that  $\bar{\alpha}$  measurements are increased (shifted upward on plots of  $\bar{\alpha}$  versus  $d$ ) and discrete  $\alpha$  measurements scatter only above the quiescent  $\alpha$  value. As a result of this modal preference, for certain values of  $d$  observations of  $\bar{\alpha}$  are shifted from the quiescent  $\alpha$  to varying degrees. This phenomenon complicates efforts to increase the accuracy of the dual-polarization technique, which relies on a predictable  $\bar{\alpha}$  versus  $d$  relationship.

Based on photographic measurements of raindrops, Beard and Kubesh (1991) proposed three oscillation regimes, or ranges of  $d$  where strong modal preferences result in distinct shifts of  $\bar{\alpha}$ . As noted previously,  $d < 1$  mm drops exhibit scant, if any, oscillation distortion so

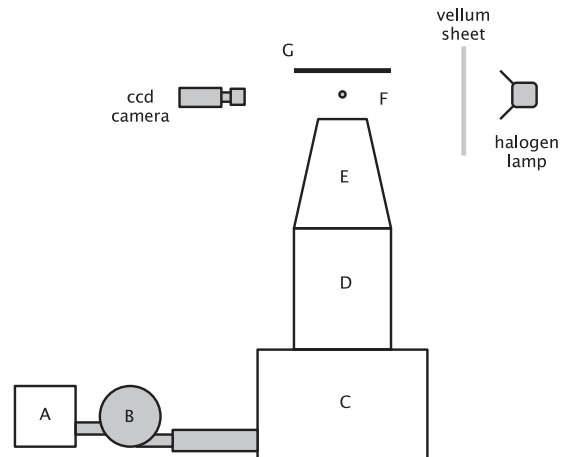


FIG. 2. Schematic of DLT.

that measurements of  $\bar{\alpha}$  agree with the quiescent shape. For drop sizes where  $d = 1$ –1.3 mm, however, a distinct upward shift in  $\bar{\alpha}$ , with  $\alpha$  measurements scattering only above the quiescent, indicates a preference for the transverse mode exclusively. Larger drops ( $d > 1.3$  mm) exhibit a similar upward shift in  $\bar{\alpha}$ —indicating the presence of the transverse mode—but with  $\alpha$  measurements scattered both above and below the quiescent, indicating the additional presence of the axisymmetric mode. These modal regimes and their implication for the dual-polarization technique have been the subject of significant work in the literature aimed at establishing the mechanism(s) of raindrop oscillations and the cause of this selective shift in  $\bar{\alpha}$ .

## 2. Apparatus

Drops were observed in the drop levitation tunnel (DLT) wind tunnel facility described by Saylor and Jones (2005) and illustrated in Fig. 2. This facility is similar to the designs from Blanchard (1950) and Kamra et al. (1986) and utilizes a stagnation plate (G) and open test section (F) to create a region of airflow favorable for the vertical levitation and observation of liquid drops. Also shown in Fig. 2 are the intake filter panels (A);  $1/4$  horsepower (HP) 25.4-cm-diameter blower (B); settling chamber (C); and a flow-conditioning section, which housed a high efficiency particulate air (HEPA) filter, honeycomb panel, and four metal screens.

As in the experiments of Blanchard (1950) and Kamra et al. (1986), an additional screen was placed at the exit of the contraction section (E) to condition the test section airflow (F). This screen incorporated an arrangement of wires stretched across a thin frame such that all of the wires crossed one another at a central point. A velocity decrement in the downstream wake of the crossed wires

served to stabilize and centrally locate levitated drops horizontally within the test section (F). This decrement is readily observed in the velocity profile presented in Fig. 3.

The downstream boundary of the test section was formed by a flat plate placed perpendicular to the flow direction (G). Selective adjustment of the height of this plate allowed for fine adjustment of the flow velocity within the test section and the levitation of a variety of drop sizes. Additional adjustment of the test section air velocity was achieved by moving a shutter at the blower inlet, which reduced or expanded the blower inlet area.

Drops were introduced into the tunnel test section through a centrally located hole in the stagnation plate (G). A drop generation apparatus protruded through the hole and was used to produce drops of varying size. The apparatus utilized compressed air to separate pendant drops from the tip of a needle, which was connected via flexible tubing to a handheld syringe so that drops were formed by manual pressure. The needle was fixed concentrically within a section of tubing that was connected to a compressed air supply so that drops were entrained within the compressed airflow and separated from the needle. Variations in drop size were achieved through careful adjustment of the size of the pendant drop and the pressure of the compressed air; an increase in pressure was required as the drop size decreased.

This drop generator was used to produce only the smallest drops that were levitated in the wind tunnel, typically in the range from  $d \approx 1.3$  mm to  $d \approx 2$  mm. Larger drops were of sufficient mass to fall from the needle under their own weight without the aid of compressed air; variation in the sizes of drops larger than  $d \approx 2$  mm was achieved by adjusting the gauge size of the drop generator needle, typically from 10–15 ga.

Although smaller drops could be produced by the drop generator, a lower size limit of drops that could be levitated in the tunnel occurred at  $d \approx 1.3$  mm as a result of the airflow from the drop generator. To create smaller droplets, it was necessary to progressively increase the air pressure in the drop generator. Consequently, these smaller drops acquired more downward momentum as they were blown from the tip of the needle. Below  $d \approx 1.3$  mm, this increase in downward momentum could not be overcome by the upward airflow of the tunnel, and drops smaller than this size fell through the upstream boundary of the test section into the contraction section of the tunnel.

Camware image acquisition software was used with a function generator to trigger a Cooke Corporation SensiCam high-speed charge-coupled device (CCD) camera. Multiple exposures (each exposure ranged from 100 to 400  $\mu$ s) were obtained of the same levitated drop as it moved slightly within the test section. This technique

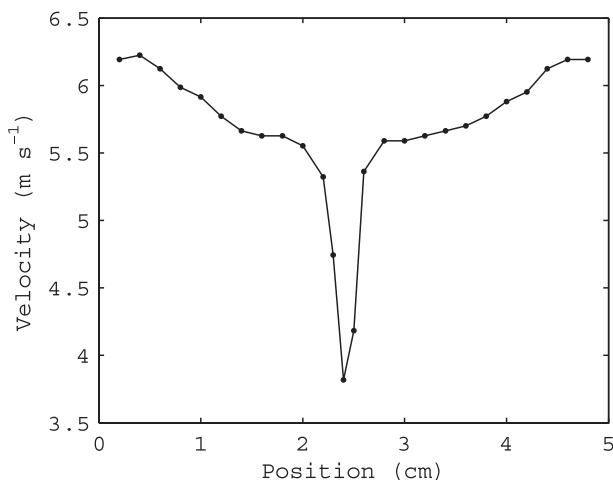


FIG. 3. Pitot-tube measurements of the DLT test section velocity profile taken 7 cm downstream of the velocity-well screen at the highest airflow setting. The valley indicates a 64% velocity decrement in the horizontal center of the test section.

produced a single image of superimposed multiple exposures. A sample image is presented in Fig. 4.

For the image data presented here, drops were illuminated using the lighting arrangement shown in Fig. 2. The setup utilized two Lowe Totalite 750-W halogen lights placed along the optical axis behind a 61.4 cm  $\times$  92.2 cm sheet of drafting vellum. Images of drops obtained using this setup appear as dark objects on a bright, diffuse background. The resulting contrast yielded images whose pixel histograms were well suited for digital drop measurement within the image analysis program described in section 3.

### 3. Experimental procedure

Images were obtained by first starting the tunnel and allowing it to operate for a short warm-up period. After this period had passed, reliable drop levitation was achieved by adjustment of the tunnel airflow through modification of the blower shutter position and stagnation plate height. The horizontal positions of the velocity-well screen and stagnation plate orifice also affected the reliability of drop levitation and required careful adjustment through trial and error. Although unsuccessful levitation attempts resulted in drops being ejected from the test section, levitated drops appeared to settle into a near-equilibrium region of airflow where they either remained perfectly stationary or erratically bounced 1–2 cm horizontally and/or vertically.

Proper camera position and focus were achieved using a finescaled rule placed in the horizontal center of the test section at the drop levitation height. Each time the camera was moved or otherwise adjusted this rule was

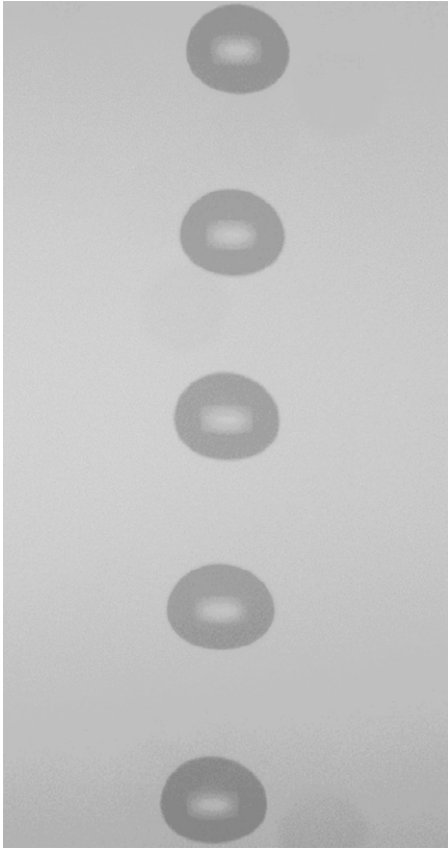


FIG. 4. Typical images obtained using the lighting arrangement shown in Fig. 2.

reimaged to obtain the correct pixel-to-millimeter magnification ratio. The camera positions and two lenses—Nikkor 105-mm 1:2.8 and Nikkor 200-mm 1:4—used during imaging resulted in four magnification ratios  $M$  of 50, 38, 36, and 22 pixels per millimeter.

After all wind tunnel and camera adjustments had been made, multiple exposure images were obtained of levitated drops, which is similar to those shown in Fig. 4. The number of multiple images of the same drop that could be obtained was determined by the time duration of levitation. This time varied with  $d$  from 2 s for the smallest drops ( $d \approx 1.3$  mm) to 1 min or longer for larger drops ( $d > 2$  mm).

After acquisition, the multiple exposure sequences were manually cropped, and each exposure in the sequence saved as a single image. MATLAB measurements of the drop in each cropped image were obtained using an algorithm that first thresholded (converted to binary, or black and white) the image according to a characteristic of its gray-level pixel histogram. This characteristic was obtained by smoothing the histogram (i.e., replacing each bin value with an average of that value and its two neighbors). A typical smoothed histogram is presented

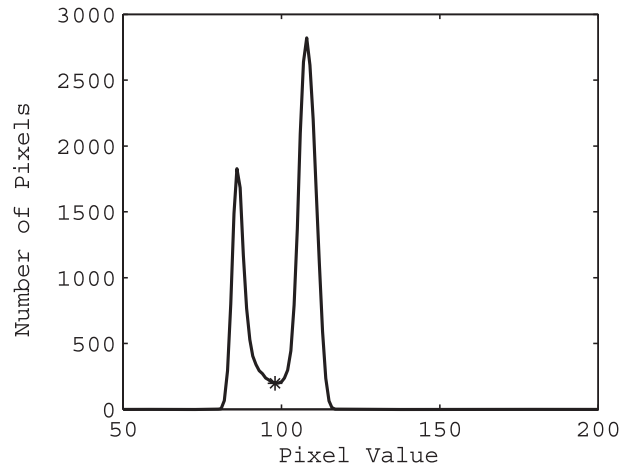


FIG. 5. Typical raw image (smoothed) histogram. The calculated threshold value is denoted by an asterisk. Lower pixel values represent darker colors.

in Fig. 5; the characteristic bimodal shape of this histogram is typical for the lighting arrangement described above.

The threshold value (i.e., the value above which all pixels were set to white and below were set to black) was chosen by identifying the minimum pixel value between the two peaks in the smoothed histogram. This minimum value was always well defined, and careful focusing of the camera lens made the value more distinct. Thus, a binary version of the image was produced from the original grayscale image. An outline of the drop was then obtained by identifying all pixels for which the pixel value changed from 0 to 1 or vice versa. The original, binary, and outlined versions of a sample drop image are presented in Fig. 6.

Once the drop outline was obtained, the drop volume was computed using an integration technique where each horizontal pixel row of the two-dimensional drop outline is assumed to correspond to the diameter of a three-dimensional disk of one pixel-height thickness. The volumes of these disks were summed to obtain a total drop volume  $V$ , from which  $d$  was obtained according to

$$D_{\text{eq}} = 2 \left( \frac{3V}{4\pi} \right)^{1/3}. \quad (3)$$

Finally, the axis ratio  $\alpha$  was computed based on the height  $h$  and width  $w$  of the drop outline according to Eq. (2).

#### 4. Results

Measurements of  $\alpha$  and  $d$  were obtained from 968 drop images. A plot of these data appears in Fig. 7 along with the  $\alpha$  of the quiescent drop shapes from Beard and Chuang (1987), which is determined according to

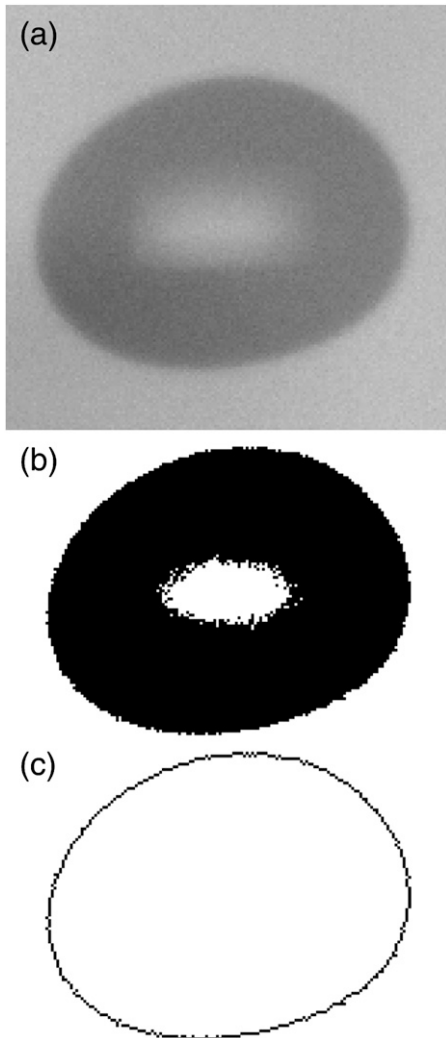


FIG. 6. (a) Raw image of a typical drop, (b) the thresholded (binary) version of this image, and (c) the outline of the drop obtained using the method described in the text.

$$\alpha = 1.0048 + 0.0057d - 2.628d^2 + 3.682d^3 - 1.677d^4. \quad (4)$$

The wide scatter in the data presented in Fig. 7 results from shape variations—presumably because of oscillations—of equivolume drops; however, the apparent striations in the data are due to quantization error in measurements of  $v$  and  $h$  because of the finite resolution of the CCD camera. This resolution was 20.0, 26.3, 27.8, or 45.5  $\mu\text{m}$  per pixel, depending on the magnification ratio  $M$  resulting from the lens and camera position associated with a particular image. The arc shape of these striations and the distinct jumps in  $\alpha$  that separate the striations themselves result from the discrete changes in  $\alpha$  and  $d$  that result from discrete jumps in either  $v$  or  $h$  or in both.

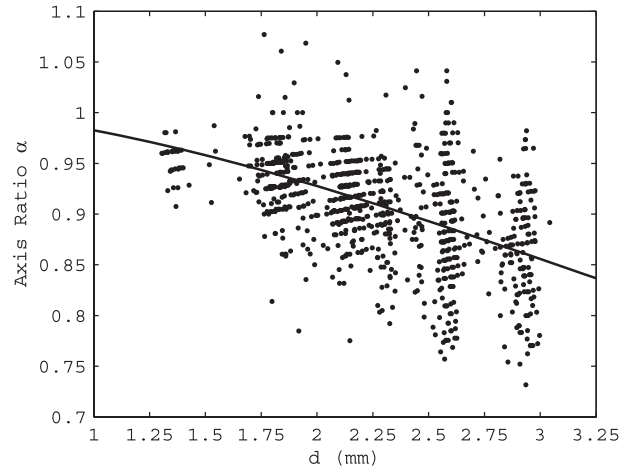


FIG. 7. Plot of all  $\alpha$  vs  $d$ . The quiescent model from Beard and Chuang [1987, their Eq. (4)] is also included and is plotted as a solid line.

All of the data presented in Fig. 7 were sorted into bins according to  $d$ . Presented in Table 1 are the average  $d$  measurement for each bin  $\bar{d}$ , the range of  $d$ , the number of drop images, and  $\bar{\alpha}$  of each of these 15 bins. Each bin spans a  $d$  range of 90  $\mu\text{m}$ , with the exception of bins 1 and 2. Because of the reduced number of imaged small diameter drops, these bins are slightly larger: 120 and 170  $\mu\text{m}$ , respectively.

A plot of  $\bar{\alpha}$  versus  $d$  is presented in Fig. 8, in which  $\bar{d}$  is shown with the quiescent  $\alpha$  from Beard and Chuang (1987). Additionally, the standard deviation of the present  $\alpha$  data for each bin  $\sigma_\alpha$  is indicated by a horizontal tick mark and the 95% confidence interval of  $\bar{\alpha}$  by a solid black square. This figure also shows the axis ratio amplitude  $\langle \alpha \rangle$  of each bin, which is defined as

$$\langle \alpha \rangle = \alpha_{\max} - \alpha_{\min}, \quad (5)$$

where  $\alpha_{\max}$  and  $\alpha_{\min}$  give the maximum and minimum  $\alpha$  of each bin, respectively. These amplitudes are depicted as the vertical bars plotted with each  $\bar{\alpha}$  and serve as an indicator of oscillation amplitude. The data agree with the quiescent model  $\alpha$  with 95% confidence, except for bin 1. This result was unexpected and will be further discussed in section 5.

## 5. Discussion

The most striking characteristic of the present data, which are shown in Fig. 8, is a lack of evidence of transverse oscillations. This evidence is normally manifested as an upward shift in  $\bar{\alpha}$  from the quiescent  $\alpha$ , and it is widely accepted that  $\bar{\alpha}$  measurements of raindrops or water drops at terminal velocity will exhibit some amount of upward shift because of transverse oscillations. Although the present data differ in this respect from observations of

TABLE 1. Drop measurement details.

Bin No.	$\bar{d}$ (mm)	$d$ range (mm)	No. of images	$\bar{\alpha}$	$\sigma_{\alpha}$
1	1.36	1.30–1.42	34	0.9530	0.0168
2	1.62	1.52–1.69	10	0.9534	0.0253
3	1.77	1.70–1.79	57	0.9402	0.0360
4	1.84	1.80–1.89	126	0.9394	0.0324
5	1.94	1.90–1.99	46	0.9234	0.0480
6	2.07	2.00–2.09	45	0.9170	0.0392
7	2.15	2.10–2.19	159	0.9171	0.0388
8	2.26	2.20–2.29	67	0.9036	0.0456
9	2.33	2.30–2.39	52	0.8952	0.0419
10	2.45	2.40–2.49	39	0.9034	0.0581
11	2.57	2.50–2.59	118	0.8864	0.0627
12	2.62	2.60–2.69	63	0.8828	0.0579
13	2.74	2.70–2.79	13	0.8874	0.0383
14	2.86	2.80–2.89	45	0.8605	0.0419
15	2.94	2.90–3.04	94	0.8601	0.0598

raindrops in the field and water drops at terminal velocity in the laboratory, these differences support the recent findings of Testik et al. (2006) and Szakáll et al. (2009) and also shed new light on previous data regarding the oscillation behavior of small- to moderate-sized drops.

The lateral drift of drops in free-fall was first observed by Gunn and Kinzer (1949) in his laboratory study of drop terminal velocity. Other drop fall tower studies have identified the phenomenon (most recently, Tokay et al. 2000). Observations of spheres and bubbles at similar Reynolds number further suggest a lateral or spiraling component of free-fall trajectory, and flow visualization studies have linked periodic wake structures to this lateral component of drop free-fall (Beard et al. 1991). This drift is problematic in experiments aimed at imaging drops at the base of tall fall towers because the drops tend to drift away from the camera field of view by the time they reach the base of the tower. These studies sometimes sought to reduce this drift by isolating the falling drops from wind currents using narrow tubes; nevertheless, drops seemed to collide with the tube walls in midfall. The phenomenon was particularly problematic in studies aimed at imaging smaller drops to the extent that the fall tower has been largely abandoned for purposes of small drop imaging (Tokay et al. 2000).

Testik et al. (2006) visualized raindrops oscillating in the transverse mode while simultaneously exhibiting this sideways drift, providing evidence of a causal relationship between the two phenomena. This result is the first to utilize high-speed imaging to establish such a correlation. They presented image sequences of oscillating falling drops exhibiting shapes characteristic of the transverse mode while simultaneously drifting sideways with 20%–30% of their downward terminal velocity. Drops that fell strictly in the vertical direction

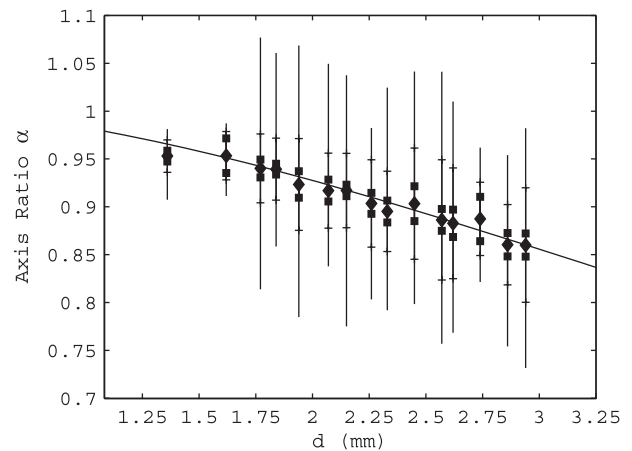


FIG. 8. Plot of mean axis ratio  $\bar{\alpha}$  vs  $d$ . The standard deviation of  $\alpha$  for each bin ( $\sigma_{\alpha}$ ) and the 95% confidence interval of  $\bar{\alpha}$  are indicated by tick marks and solid black squares, respectively. Axis ratio amplitudes ( $\alpha$ ) are represented by the extent of vertical lines. The model from Beard and Chuang (1987) is also shown.

exhibited an axisymmetric shape change from image to image, which further suggests a positive correlation between oscillation mode and fall trajectory.

The present data support a similar link. Because the drop levitation tunnel employed an upward directed airflow in the direction opposite gravity, the test section of the tunnel simulated only strictly vertical free-fall. The data shown in Fig. 8 appear to indicate that this airflow was only appropriate for axisymmetric-oscillating drops or quiescent drops because of the absence of transverse oscillations. Stated differently, when the results of Testik et al. (2006) are considered in this context, it seems that transverse-oscillating drops were rejected from the test section, because flow conditions were inappropriate to simulate free-fall for these drops. In addition to the reduction in  $\bar{\alpha}$  the reduction in  $\sigma_{\alpha}$  and  $\langle\alpha\rangle$  shown in Fig. 8 for  $d = 1.3$  mm may indicate a reduction in oscillations at these sizes, further suggesting that the few drops that were imaged were simply quiescent or axisymmetric oscillating. That the current observations deviate with such significance from the literature seems to indicate that smaller-sized drops prefer transverse mode oscillations.

The  $\alpha$  measurements from Andsager et al. (1999) also show the absence of a shift in  $\bar{\alpha}$  and thus an absence of transverse oscillations. They suggest that perhaps a steady-state condition arises some time after drops reach terminal velocity, and this condition is necessary for the exhibition of transverse oscillations and the shift in  $\bar{\alpha}$  that they affect. These authors further posit an oscillation mechanism where the axisymmetric mode is most common, but the periodic shedding of vortices at terminal velocity gradually forces transverse oscillations that increase in amplitude via resonance with surface tension and aerodynamic forces.

Disturbances from equilibrium during drop levitation could be to blame for the absence of transverse oscillations and the predominance of axisymmetric oscillations in the present data. As mentioned previously, erratic vertical movements during levitation indicate repeated slight deviations from a precise equilibrium condition. Perhaps these disturbances prevented attainment of the steady-state condition described by Andsager et al. (1999), regardless of the time duration of levitation. In this way, the present data further support a steady-state aerodynamic effect as the cause of the upward shift in  $\bar{\alpha}$  measurements of small raindrops.

Additional explanation of the current data may be found in the recent work of Szakáll et al. (2009). They present measurements of 56 water drops obtained using a wind tunnel designed to minimize turbulent velocity fluctuations and shear, perhaps the cause of the equilibrium disturbances in the wind tunnel used here. However, the authors report an absence of any shift in mean axis ratio in spite of their flow-conditioning techniques. Although the present data only overlap those of Szakáll et al. (2009) in the  $d = 2.5\text{--}3.0$  mm size range, the result is similar to the present work in its discordance with the literature with respect to the upward shift in mean axis ratio.

In both cases, perhaps the lack of observation of transverse oscillations resulted from the tendency of these drops to prefer nonvertical fall trajectories, because transverse-oscillating drops drifted laterally away from the camera field of view. Even if these drops were briefly imaged and their axis ratios measured—Szakáll et al. (2009) note difficulties with levitation and imaging of small drop sizes ( $d < 2.5$  mm) and short levitation times for other drops ( $< 2$  s)—perhaps a greater number of images (and axis ratio measurements) were obtained of axisymmetric-oscillating drops because of the more stable nature of their levitation. If true, such a sampling bias could explain the lack of a mean axis ratio shift. Although it is tempting to conclude the nonexistence of a mean axis ratio shift in natural raindrops from both results, perhaps transverse oscillating drops were simply underrepresented in the observations of both wind tunnel studies. To more accurately characterize the extent and nature of the mean axis ratio shift, a high-speed imaging system incorporating a wide field of view may be best, so that the lateral motions resulting from transverse oscillations do not exclude these drops from axis ratio measurement data.

## 6. Conclusions

Axis ratio measurements of water drops at terminal velocity were obtained via high-speed imaging of drops levitated in a vertically oriented wind tunnel. Although drop oscillations were inferred from the data, transverse

oscillations were markedly absent. This result was unexpected, because the published data typically show a shift in  $\bar{\alpha}$ , which indicates the presence of these oscillations. It is postulated that aerodynamic conditions inherent to the wind tunnel design were such that drops oscillating in the transverse mode were rejected from the tunnel test section and were not imaged. This conclusion suggests that the present data agree with recent observations indicating transverse oscillating drops necessarily drift laterally from a true vertical trajectory.

*Acknowledgments.* This work was supported by the South Carolina Space Grant Consortium, a NASA funded agency.

## REFERENCES

- Andsager, K., K. Beard, and N. Laird, 1999: Laboratory measurements of axis ratios for large raindrops. *J. Atmos. Sci.*, **56**, 2673–2683.
- Beard, K. V., and C. Chuang, 1987: A new model for the equilibrium shape of raindrops. *J. Atmos. Sci.*, **44**, 1509–1524.
- , and R. J. Kubesh, 1991: Laboratory measurements of small raindrop distortion. Part 2: Oscillation frequencies and modes. *J. Atmos. Sci.*, **48**, 2245–2264.
- , —, and H. T. I. Ochs, 1991: Laboratory measurements of small raindrop distortion. Part I: Axis ratios and fall behavior. *J. Atmos. Sci.*, **48**, 698–710.
- Blanchard, D. C., 1950: The behavior of water drops at terminal velocity in air. *Trans. Amer. Geophys. Union*, **31**, 836–842.
- Chandrasekar, V., W. A. Cooper, and V. N. Bringi, 1988: Axis ratios and oscillations of raindrops. *J. Atmos. Sci.*, **45**, 1323–1333.
- Doviak, R. J., and D. S. Zrnic, 1984: *Doppler Radar and Weather Observations*. Academic Press, 486 pp.
- Gunn, R., and G. D. Kinzer, 1949: The terminal velocity of fall for water droplets in stagnant air. *J. Meteor.*, **6**, 243–248.
- Kamra, A. K., A. B. Sathe, and D. V. Ahir, 1986: A vertical wind tunnel for water drop studies. *Mausam*, **37**, 219–222.
- Marshall, J. S., and W. Palmer, 1948: The distribution of raindrops with size. *J. Meteor.*, **5**, 165–166.
- Musgrove, C., and M. Brook, 1975: Microwave echo fluctuations produced by vibrating water drops. *J. Atmos. Sci.*, **32**, 2001–2007.
- Rayleigh, L., 1879: On the capillary phenomenon of jets. *Proc. Roy. Soc. London*, **21**, 71–97.
- Saylor, J. R., and B. K. Jones, 2005: The existence of vortices in the wakes of simulated raindrops. *Phys. Fluids*, **17**, 031706, doi:10.1063/1.1874192.
- Szakáll, M., K. Diehl, S. K. Mitra, and S. Borrmann, 2009: A wind tunnel study on the shape, oscillation, and internal circulation of large raindrops with sizes between 2.5 and 7.5 mm. *J. Atmos. Sci.*, **66**, 755–765.
- Testik, F. Y., A. P. Barros, and L. F. Bliven, 2006: Field observations of multimode raindrop oscillations by high-speed imaging. *J. Atmos. Sci.*, **63**, 2663–2668.
- Tokay, A., R. Chamberlain, and M. Schoenhuber, 2000: Laboratory and field measurements of raindrop oscillations. *Phys. Chem. Earth*, **25B** (10–12), 867–870.
- Ulbrich, C. W., 1986: A review of the differential reflectivity technique for measuring rainfall. *IEEE Trans. Geosci. Remote Sens.*, **24**, 955–965.

Copyright of *Journal of Atmospheric & Oceanic Technology* is the property of *American Meteorological Society* and its content may not be copied or emailed to multiple sites or posted to a listserv without the copyright holder's express written permission. However, users may print, download, or email articles for individual use.